Available online at www.sciencedirect.com
ScienceDirect
Journal of Catalysis 250 (2007) 209–221
JOURNAL OF CATALYSIS
www.elsevier.com/locate/jcat

Dodecane reforming over nickel-based monolith catalysts

Benjamin D. Gould, Xiaoyin Chen, Johannes W. Schwank *

Transportation Energy Center, Department of Chemical Engineering, University of Michigan, Ann Arbor, MI 48109, USA

Received 30 April 2007; revised 13 June 2007; accepted 17 June 2007

Available online 30 July 2007

Abstract

Autothermal reforming (ATR) of *n*-dodecane was systematically investigated with O/C = 0.6 and $H_2O/C = 2.0$ over nickel-based catalysts supported on cordierite monoliths. Both nickel supported on monolith (Ni/monolith) and nickel supported on cerium–zirconium oxide (CZO) loaded on monolith (Ni/CZO/monolith) were tested for ATR activity. The influence of nickel weight loading (0–16 wt%) on ATR product yields was examined. Experimental results showed that 2 wt% Ni/CZO/monolith was an optimal composition for ATR. The roles of Ni and CZO were determined by comparing *n*-dodecane conversion, oxygen conversion, the extent of reforming, and product yields (i.e., CO, CO_2, and H_2). The reaction studies indicated that nickel catalyzed the conversion of *n*-dodecane by POX and SR, yielding a hydrogen rich effluent, whereas CZO alone catalyzed the conversion of *n*-dodecane though catalytic oxidation and cracking, yielding an effluent rich in smaller hydrocarbon species. Nickel supported on CZO showed the greatest hydrogen, carbon monoxide, and carbon dioxide yields of the catalysts studied. ATR, partial oxidation (POX), steam reforming (SR), and the influence of reaction temperature on ATR were studied separately and compared at similar conditions over 2 wt% Ni/monolith and 2 wt% Ni/CZO/monolith to elucidate the primary reforming reactions. An *n*-dodecane ATR reaction schematic is postulated, and the influences of homogeneous activity and oxygen conversion are discussed. It is proposed that POX, homogeneous cracking, and oxidative cracking are the major routes for *n*-dodecane conversion during ATR, whereas POX of *n*-dodecane and SR of smaller hydrocarbons are the primary routes to reforming products (i.e., H_2, CO, and CO_2).

Keywords: Autothermal reforming; Partial oxidation; Steam reforming; Ceria–zirconia: monolith; Dodecane; Jet fuel; Diesel fuel; Nickel

1. Introduction

The ability to process liquid hydrocarbons into carbon monoxide and hydrogen onboard of a vehicle is very desirable, because reformate is needed as a fuel for solid oxide fuel cells and as a reducing agent for catalytic emissions control [1–3]. One of the major technological barriers preventing the implementation of onboard fuel reforming is the activity and durability of current liquid hydrocarbon-reforming catalysts. The activity of liquid hydrocarbon-reforming catalysts is compromised by carbon deposition and sulfur poisoning associated with the processing of heavier hydrocarbon fuels. Hydrocarbons larger than those found in gasoline are of particular interest because of their potential application in military and diesel freight vehicles. One particularly exciting application of on-board fuel reforming technology is in auxiliary power units (APUs), which can increase fuel economy by displacing engine idling. Vehicular applications require that catalysts be supported on engineered substrates to avoid the physical attrition that plagued packed beds in early emissions control catalysis [4].

The two primary catalytic processes for converting hydrocarbons into carbon monoxide and hydrogen are steam reforming (SR) and partial oxidation (POX). Autothermal reforming (ATR) is a hybrid process that combines the exotherm of POX to drive the endotherm in SR. The presence of reforming products makes the water–gas shift reaction possible during reforming and is often considered equilibrated at reforming temperatures. The three hydrocarbon reforming reactions and the water–gas shift reaction are

$$C_nH_m + \tfrac{1}{2}nO_2 \rightarrow nCO + \tfrac{1}{2}mH_2, \quad (1)$$

$$C_nH_m + nH_2O \rightarrow nCO + \left(n + \tfrac{1}{2}m\right)H_2, \quad (2)$$

* Corresponding author.
E-mail addresses: gouldb@umich.edu (B.D. Gould), xychen@umich.edu (X. Chen), schwank@umich.edu (J.W. Schwank).

0021-9517/$ – see front matter
doi:10.1016/j.jcat.2007.06.020

$$C_nH_m + xO_2 + (n-2x)H_2O \rightarrow nCO + \left(n-2x+\tfrac{1}{2}m\right)H_2, \quad (3)$$

and

$$CO + H_2O \leftrightarrow CO_2 + H_2. \quad (4)$$

Equation (3) is an idealized reaction assuming that ATR is a simple combination of reactions (1) and (2). However, ATR is often described by a reaction producing CO_2 instead of CO [5,6]. In reality, ATR produces both CO and CO_2, due to the presence of excess water providing a pathway for the water–gas shift [Eq. (4)] [5]. We studied all of these reforming reactions separately under comparable reactor conditions over a range of nickel-based catalysts.

POX and SR are thought to proceed sequentially during ATR, with POX occurring first, followed by SR [7,8]. SR and POX mechanistic studies have focused primarily on methane because of its simplicity and importance to industrial hydrogen production from natural gas. SR of methane is believed to proceed though C–H bond activation [9,10]. Whether POX of methane proceeds by a direct or indirect mechanism is a matter of debate [11–13]. However, there is no comprehensive mechanism for ATR of light hydrocarbons, let alone hydrocarbons larger than C_8 [14]. Although mechanistic understanding of ATR of large hydrocarbons remains sparse, great progress has been made in catalyst development and reactor operation.

ATR of liquid hydrocarbons in the C_8–C_{16} range has been studied over various supported metals, including Ni [15–18], Pt [17–21], Ru [17], Rh [8,20], Pd [17], Fe [17], and Co [17]. Precious metals, particularly platinum, supported on ceria seem to be the materials of choice for larger hydrocarbon reforming [22–26]. Support materials with oxygen storage capacity, usually ceria or cerium–zirconium oxide (CZO), are attractive because of their redox properties used in automotive emissions catalysis. It has been suggested the ceria plays a role in POX though a redox mechanism [27]. Others have suggested that the role of ceria is to prevent carbon formation [28]. Most studies have been on catalysts in powder form, with relatively few studies on engineered substrates. Nickel has shown relatively high activity and product selectivity for ATR compared with precious metals [17]. Although nickel has poorer performance than precious metals, nickel is roughly three orders of magnitude less expensive than platinum. This makes nickel an attractive catalytic option if durability can be managed though metal loading, support choice, and reforming conditions.

One of the most important differences between the reforming of large straight-chained alkanes (*n*-dodecane) and smaller branched alkanes (isooctane) is their autoignition temperatures and boiling points. Isooctane's autoignition temperature of 415 °C is nearly twice that of *n*-dodecane (204 °C). Vaporization of larger hydrocarbon fuels under ATR conditions is difficult because their boiling points (e.g., 215 °C for *n*-dodecane) are higher than their autoignition temperatures [29]. This makes homogeneous combustion of large hydrocarbons possible, depending on reactant concentrations.

In previous work done in our laboratories, we found that a 10 wt% Ni/$Ce_{0.75}Zr_{0.25}O_2$ powder catalyst was very active in converting *n*-dodecane and tetralin into reforming products [30]. Encouraged by our work on powder Ni/$Ce_{0.75}Zr_{0.25}O_2$ catalysts, a suite of nickel-only and nickel/ceria–zirconia catalysts supported on cordierite monoliths were prepared and tested for reforming activity. The roles of nickel and CZO were studied under ATR, SR, and POX conditions. Few previous studies have compared ATR and its constituent reactions [31,32]. To the best of our knowledge, this may be the first experimental comparison in which all three reactions (ATR, POX, and SR of *n*-dodecane) were run separately over the same catalyst under comparable reaction conditions. In addition, the influence of nickel loading was also studied and optimized.

The objective of this paper is to elucidate the roles of nickel and CZO during ATR. Insights gained will contribute to further the development of nickel-based catalytic materials for mobile liquid fuel reforming. The ultimate goal of our work is the development of a robust liquid fuel ATR catalyst capable of processing jet and diesel fuels.

2. Experimental

2.1. Catalyst synthesis

A series of catalysts based on the composition of $Ce_{0.75}Zr_{0.25}O_2$ (0 and 23 wt%) and nickel (0–16 wt%) loadings were prepared by solution coating and wet impregnation. Cylindrical cordierite monoliths (15.3 cm diameter, 7.6 cm tall, 400 cpsi cell density) were obtained from Dow Corning. The large cordierite cylinders were cut into smaller sample cylinders 2.5 cm tall and 1 cm in diameter. These sample monoliths were then washed thoroughly in DI water, dried in an oven at 110 °C overnight, and calcined at 600 °C in air for 4 h before solution coating.

Typically, the solution coating of CZO was carried out by multiple immersions of the monolith into an aqueous solution of $Ce(NO_3)_3{\cdot}6H_2O$ and $ZrOCl{\cdot}8H_2O$. Between each immersion, excess solution was blown out of the cell channels with purified compressed air. The wetted monoliths were dried at room temperature overnight and then dried in an oven at 110 °C for 2 h. After drying, the cerium–zirconium precursors were oxidized by a final calcination in air at 600 °C for 2 h. This coating procedure was repeated until a target CZO weight loading was reached. The loading of the nickel phase was accomplished by immersing the CZO-coated monolith into an aqueous solution of $Ni(NO_3)_2{\cdot}6H_2O$, followed by drying and calcination in air at 600 °C.

2.2. Flow reactor experiments

All reaction experiments were carried out in a horizontal quartz flow reactor system. The detailed description of equipment specifications and reactor dimensions was described previously [30]. The basic setup consisted of an Instech peristaltic pump for water delivery, an Isco syringe pump for fuel delivery, a 10-m section of stainless steel tubing wrapped with heating tape to vaporize the liquids, and a 200-mL ice water-cooled condenser. Incoming gas flows were metered with MKS

mass flow controllers. Monoliths were placed in the center of the quartz tube and, when necessary, wrapped with Nobest™ ceramic tape to remove any dead space between the monolith and the reactor wall that might cause gas channeling. Thermocouples were placed 2–3 mm in front and behind the monolith catalysts to ensure that none of the channels were blocked by the thermocouples. Before reaction, the monolith catalysts were aged in 100 sccm of air at 800 °C. This temperature was greater than most of the temperatures encountered during reforming and ensured that the catalyst surface areas remained thermally stable during reaction. After aging, the catalysts were cooled to 600 °C in flowing N_2 and reduced in a 100-sccm stream of 5% H_2/N_2 for 1 h. The reactor was then cooled to room temperature under a 100-sccm N_2 flow.

In this work, *n*-dodecane was used as single component fuel surrogate to represent jet fuel. The *n*-dodecane was purchased from Sigma Aldrich (>99% purity). A constant molar flow rate of *n*-dodecane was used in each set of experiments (0.132 mol $C_{12}H_{26}$ h^{-1}). The space velocity was calculated using the total geometric volume of the catalyst cylinder and held constant at 63,000 h^{-1} in all of the experiments. Fresh monolith catalyst samples were used at each experimental condition. An oxygen-to-carbon ratio of 0.6 and a steam-to-carbon ratio of 2.0 were used in all of the reaction experiments where relevant; POX did not have a steam-to-carbon ratio. These conditions were chosen so that catalysts could be studied under incomplete conversion of the *n*-dodecane and so that a substantial portion of the incoming fuel had to be converted by SR under ATR conditions. This is in contrast to typical ATR conditions reported in most studies, in which an oxygen-to-carbon ratio of 1.0 was used. In these cases, the amount of oxygen was sufficient to cause complete conversion of hydrocarbon via POX.

The reactor effluent product compositions were analyzed by gas chromatography, using a Varian CP-3800 gas chromatograph with two thermal conductivity detectors (TCDs) and a flame ionization detector (FID). A Haysep DB column connected to a TCD operating with argon carrier gas was used to quantify the concentration of H_2 in the effluent stream. A Molesieve 13× column connected to a second TCD operating with helium carrier gas was used to quantify the concentration of O_2, N_2, CO, CO_2, and CH_4. A capillary CP-Sil 5CB column connected to the FID was used to quantify uncondensed C_2–C_4 hydrocarbon species. Quantification of olefins versus paraffins was not performed in this study, because species with the same number of carbon atoms co-eluted on the capillary column. The molar flow rates of individual species were determined from the individual effluent concentrations and total effluent flow rates. After elution of the permanent gases, the column temperature was ramped from 40 to 200 °C.

The following metrics were used to judge the performance of the monolith catalysts:

$$Y_{H_2} = \frac{F_{H_2,\text{out}}}{13 \cdot F_{C_{12}H_{26},\text{in}}}, \tag{5}$$

$$Y_{CO} = \frac{F_{CO,\text{out}}}{12 \cdot F_{C_{12}H_{26},\text{in}}}, \tag{6}$$

$$Y_{CO_2} = \frac{F_{CO_2,\text{out}}}{12 \cdot F_{C_{12}H_{26},\text{in}}}, \tag{7}$$

$$X_{REF} = \frac{F_{CO} + F_{CO_2}}{12 \cdot F_{C_{12}H_{26},\text{in}}} = Y_{CO} + Y_{CO_2}, \tag{8}$$

$$X_{O_2} = 1 - \frac{F_{O_2,\text{out}}}{F_{O_2,\text{in}}}, \tag{9}$$

and

$$X_{C_{12}} = 1 - \frac{M_{C_{12}H_{26},\text{out}}}{M_{C_{12}H_{26},\text{in}}}. \tag{10}$$

Equations (5)–(7) describe the yields of the three important reforming products (H_2, CO, and CO_2) as determined on a fuel basis. This allows for hydrogen yields greater than unity if there is significant SR activity. Equation (8) is the extent of reforming (X_{REF}) and represents how much of the carbon in the fuel ended up in reforming products (CO and CO_2). The abbreviations X_{ATR}, X_{SR}, and X_{POX} denote the specific reaction environment used during the calculation of extent of reforming. In many ways this is a better metric of performance than the conversion of the *n*-dodecane, because there are many possible routes for the conversion of *n*-dodecane that do not yield reformate, including pyrolysis and carbon deposition via the Boudouard reaction. Equation (9) was used to calculate the oxygen conversion. In Eqs. (5)–(9), F is the molar flow rate of the subscripted species in mol s^{-1}. The molar flow rate of *n*-dodecane was calculated from the pump volumetric flow rate. The flow rate of the individual product species was determined from the species effluent concentration and the total effluent flow rate on a dry basis. The conversion of *n*-dodecane ($X_{C_{12}}$) was determined as a time-weighted average over the entire experiment by weighing the organic phase in the condenser. The total mass on *n*-dodecane in the effluent condenser ($M_{C_{12}H_{26},\text{out}}$) was compared with the total mass of *n*-dodecane fed into the reactor by the syringe pump ($M_{C_{12}H_{26},\text{in}}$). The condenser's ability to capture most of the *n*-dodecane was verified by low-temperature blank runs showing *n*-dodecane recovery >99% by mass. The organic phase in the condenser was assumed to be pure *n*-dodecane. The organic phase in the condenser may have contained other hydrocarbons, and complete analysis of the organic phase was not performed. However, a few preliminary qualitative GC–MS studies of the condensate showed that *n*-dodecane was by far the largest peak in the condensate.

During the experiments at low temperature and incomplete *n*-dodecane conversion, the monolith samples showed slight to significant losses in selectivity toward reaction products during the course of the reactions [33]. The deactivation behavior and carbon formation will be subjects of future study. Because deactivation occurred at different rates over the individual catalysts, simply reporting average yields could lead to erroneous conclusions as to which catalyst formulation was initially the most active. To compare the different catalysts on a consistent time basis, the individual product yields were measured at 30-min intervals, starting 3 min after the furnace set point temperature had been reached. All of the data points were fitted by a linear function, and the y-intercept value was chosen to represent the initial yield at time zero, defined as the moment where the furnace temperature had reached the desired set point. The initial

product yields obtained by this procedure are reported with a 95% confidence interval.

2.3. Reactor startup and shutdown procedure

Initially, the monolith catalyst and reactor were heated under flowing nitrogen to a temperature of 250 °C. The flow of steam was brought on stream rapidly, followed by the flow of air. As air was introduced into the reactor, the flow of nitrogen was ceased. The flow of steam and air was given approximately 10 min to reach steady state before the fuel was introduced into the system. At this point, all of the reactants were being fed into the reactor, but the temperature was too low for any appreciable ATR or POX reactions to occur. The ATR and POX reactions were initiated by ramping the furnace temperature from 250 °C to the desired feed temperature over a period of 1 h. In most of the experiments, the feed temperature was 550 °C. In experiments comparing the influence of feed temperature on product yield, the feed temperature ranged from 550 to 950 °C. Once the reaction started, the furnace temperature was held constant to preheat the reactants. The duration of each experimental run was 4 h, after which the reaction was extinguished by turning off the air, fuel, and steam in rapid succession in an attempt to preserve the catalyst as much as possible in its operational state for accurate postreaction characterization. As the air was turned off, nitrogen was brought on stream to flush the reactor as it cooled to room temperature; this ensured that surface carbon would not be oxidized during furnace cooling.

The reactor startup procedure was modified for SR, to avoid coking during startup. The reactor was brought to 640 °C under flowing N_2, and then the steam flow was established, followed by addition of vaporized fuel.

2.4. Catalyst characterization

The specific surface areas (BET) of fresh intact monolith catalysts were characterized by a multipoint physical adsorption of nitrogen using a Micromeritics ASAP 2020 instrument (P/P_0 0.05–0.3) at 77.5 K. All samples were degassed under vacuum at 350 °C for 2 h before analysis. Hydrogen chemisorption measurements were performed using the same instrument at 35 °C. All samples were intact monoliths and were degassed at 300 °C under vacuum, followed by reduction in flowing hydrogen at 600 °C. For each sample, two complete isotherms were collected. The first isotherm gave the total uptake of hydrogen. Then the sample was evacuated, and a second isotherm was obtained to determine the amount of weakly adsorbed hydrogen. We used only the remaining strongly adsorbed hydrogen to calculate the metal dispersion. Powder X-ray diffraction (XRD) was performed using a rotating-anode Rigaku Rotaflex RU-200B series X-ray diffractometer with a CuKα source at 40 kV and 100 mA.

3. Results and discussion

3.1. BET surface areas

The surface areas and nominal weight loadings of freshly prepared catalysts after calcination in air at 600 °C are given in Table 1. All weight loadings are presented as the weight of either nickel or CZO divided by the weight of bare monolith after calcination at 600 °C. The coating of CZO onto the bare monolith greatly increased the overall surface area of the material from 0.4 to 7.0 $m^2\,g^{-1}$. For comparison, unsupported CZO powder precipitated from aqueous solutions of precursor salts had a surface area of 60–70 $m^2\,g^{-1}$ after calcination at 600 °C. The surface area of monolith loaded with CZO was 7.0 $m^2\,g^{-1}$, much lower than expected for a simple physical mixture (14.6 $m^2\,g^{-1}$) of monolith and CZO powder with the same CZO-to-monolith ratio. The deposition of CZO from a salt solution onto a monolith led to lower physical surface area compared with CZO produced during precipitation. Solution coating and precipitation probably produced CZO particles with very different morphologies, accounting for their differences in surface area. The addition of 1–2 wt% Ni to the CZO-coated monoliths led to an increase in physical surface area. Further additions of nickel (4–14 wt%) to the CZO-coated monoliths led to a general loss in surface area. In contrast, the addition of nickel to the bare cordierite monolith led to an increase in surface area. The increased surface area was likely caused by the addition of NiO particles, which have a greater surface area than cordierite. In addition, it is also conceivable that the synthesis from nitrate precursors led to roughening of the surface and greater surface area.

Table 1
Monolith catalyst compositions and specific surface areas

Sample ID	Wt% CZO (w_{CZO}/w_{mono})	Wt% Ni (w_{Ni}/w_{mono})	Fresh ($m^2\,g^{-1}$)
MN00	0	0	0.4
MN01	0	1	0.4
MN02	0	2	0.5
MN03	0	4	0.6
MN04	0	7	1.0
MN05	0	11	0.9
MN06	0	13	1.0
MCZON00	22	0	7.0
MCZON01	22	1	8.3
MCZON02	22	2	7.3
MCZON03	22	4	5.9
MCZON04	22	8	5.9
MCZON05	22	12	3.9
MCZON06	22	16	4.8

Table 2
Selected monolith catalyst compositions and properties from H_2 chemisorption

Sample ID	Wt% CZO (w_{CZO}/w_{mono})	Wt% Ni (w_{Ni}/w_{mono})	Ni SA ($m^2\,g^{-1}$)	Dispersion (%)
MCZON00	22	0	0.00	n/a
MCZON02	22	2	0.24	2.42
MCZON05	22	12	0.38	0.65
MN06	0	13	0.15	0.19

3.2. H_2 chemisorption

The results of hydrogen chemisorption for selected monolith catalysts are given in Table 2. All H_2 chemisorption measurements were performed after reaction pretreatment condi-

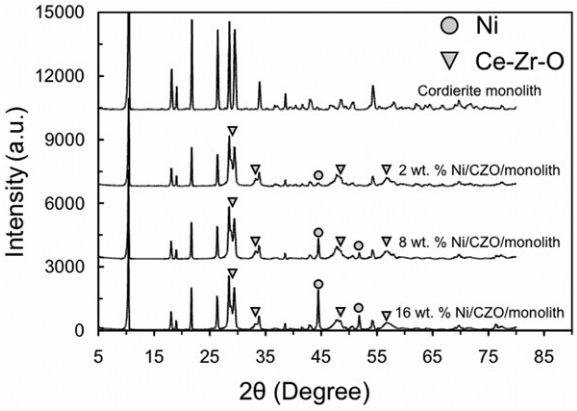

Fig. 1. X-ray diffraction patterns of cordierite monolith and Ni/CZO/monolith post-autothermal reforming.

tions, 800 °C in air for 1 h and 600 °C in 5% H_2/N_2 for 1 h. The monoliths containing only CZO but no nickel showed no measurable hydrogen chemisorption. Nickel dispersions were fairly low, <5% for all samples. As expected, the 12 wt% Ni/CZO/monolith (MCZON05) had a greater nickel surface area, but poorer nickel dispersion, than the 2 wt% Ni. In the sample without CZO (MN06), the nickel dispersion was much lower than in MCZON05, which had a comparable nickel loading. This indicates that coating the monolith with CZO is beneficial for nickel dispersion.

3.3. XRD

Powder XRD patterns of unused dried cordierite and the Ni/CZO/monolith catalysts post-ATR are shown in Fig. 1. As expected, all of the monolith catalysts showed cordierite reflections. The Ni/CZO/monolith catalysts (22 wt% CZO) showed reflections associated with CZO. For the 2 wt% Ni/CZO/monolith, a nickel metal reflection at 44.5° was barely visible above baseline. The 8 wt% and 16 wt% Ni/CZO/monolith catalysts showed strong nickel metal reflections that increased in intensity with increased nickel loading. After ATR, the nickel remained in a metallic bulk phase, and no XRD evidence for nickel oxide formation was found.

3.4. ATR

Fig. 2 compares the conversion of *n*-dodecane ($X_{C_{12}}$), the initial conversion of molecular oxygen (X_{O_2}), and the initial extent of reforming (X_{ATR}) [i.e., the conversion of *n*-dodecane to reforming products (CO and CO_2)], with respect to nickel weight loading of the monolith catalysts with and without CZO. The monoliths with no catalytic material (0 wt% Ni, 0 wt% CZO) had conversions of oxygen and *n*-dodecane of 0.33 and 0.39, respectively as shown in Fig. 2a. The conversions over bare monoliths are comparable to the conversions seen during empty quartz tube reactor studies in the literature [34]. Clearly, even under these mild reaction conditions (O/C = 0.6, $T = 550$ °C), homogeneous reactions contribute significantly to the conversion of both oxygen and *n*-dodecane.

When nickel was loaded on monolith alone (Fig. 2a), all three metrics of performance showed similar trends. Addition

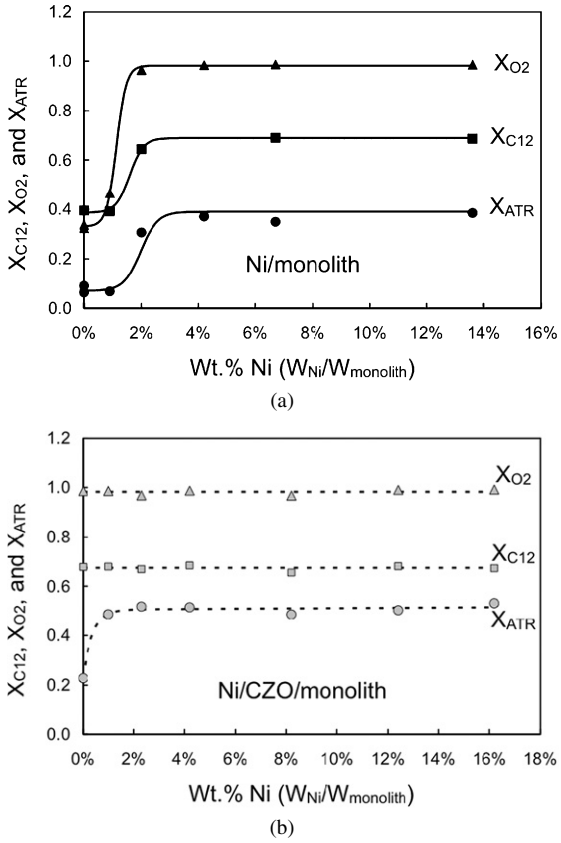

Fig. 2. Conversion of *n*-dodecane, oxygen, and the extent of reforming during autothermal reforming over (a) Ni/monolith catalysts, (b) Ni/CZO/monolith catalysts. Reaction conditions: O/C = 0.6, $H_2O/C = 2.0$, GHSV = 63,000 h^{-1}, feed temp. = 550 °C.

of 1 wt% Ni did not lead to significant increases in conversion or the extent of reforming. Adding 2 wt% nickel, however, gave a rapid increase in all three performance metrics. At a nickel loading of 4 wt%, complete conversion of oxygen was observed, and the conversion of *n*-dodecane and the extent of reforming remained constant at 0.69 and 0.39, respectively. From a conversion standpoint, nickel loadings >4 wt% Ni were superfluous. It is interesting to note that the leveling off of *n*-dodecane conversion coincided with the complete conversion of oxygen. The primary function of the nickel in the Ni/monolith catalysts was to improve the conversion of *n*-dodecane to reforming products and to increase oxygen conversion.

Unlike the Ni/monolith catalysts, the Ni/CZO/monolith catalysts (Fig. 2b) showed complete conversion of oxygen and constant conversion of *n*-dodecane ($X_{C_{12}} = 0.67$) for any given weight loading of nickel (0–16 wt%). CZO alone was a capable hydrocarbon oxidation catalyst, but without a metal component, it had poor selectivity for ATR products, as demonstrated by its low extent of reforming ($X_{ATR} = 0.23$). This observation is consistent with the well-known oxygen storage and transfer ability of ceria. Small additions of nickel led to increased extent of reforming, which leveled off after 2 wt% Ni. From an extent of reforming perspective, an optimal nickel loading was 2 wt%, because additional nickel did not change the performance. Lower nickel loadings also gave the highest physical surface areas and nickel dispersions. At complete oxygen con-

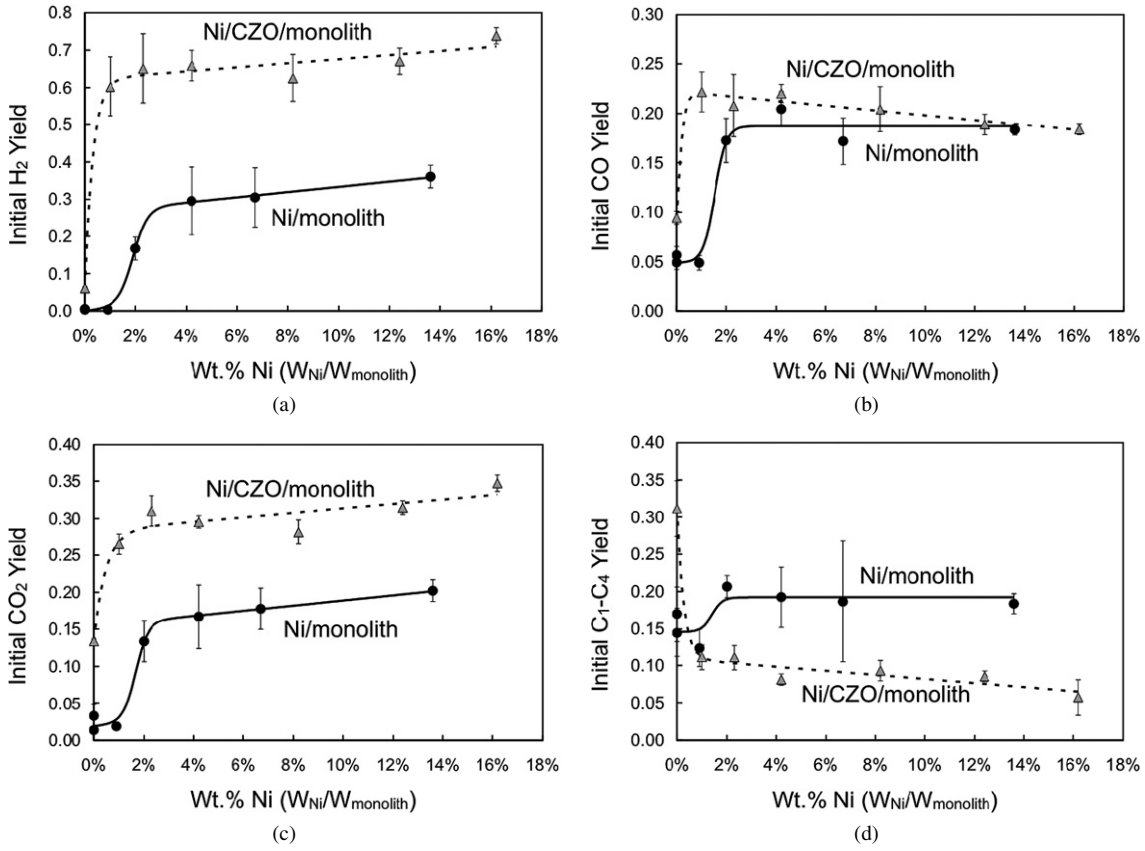

Fig. 3. Autothermal reforming of *n*-dodecane over Ni/CZO/monolith and Ni/monolith, initial product yields of (a) hydrogen, (b) carbon monoxide, (c) carbon dioxide, and (d) the total yield of C_1–C_4 hydrocarbon species. Reaction conditions: O/C = 0.6, H_2O/C = 2.0, GHSV = 63,000 h^{-1}, feed temp. = 550 °C.

versions, the Ni/CZO/monolith catalysts were superior to the Ni/monolith catalysts, giving a 31% greater extent of reforming. Interestingly, the Ni/monolith and Ni/CZO/monolith catalysts showed very similar *n*-dodecane conversions, 0.69 and 0.67, respectively, at complete oxygen conversion. The function of CZO was to increase the extent of reforming and act as an oxidation catalyst.

When the individual product yields are examined, the roles of nickel and CZO become more apparent. Fig. 3 depicts the initial product yields of the three principal reforming products (H_2, CO, and CO_2) and the total yield of smaller hydrocarbons, ranging from one to four carbons atoms (C_1–C_4). The bare monolith showed very little ATR selectivity, with a near-zero hydrogen yield (Fig. 3a), a 0.05 carbon monoxide yield (Fig. 3b), and a <0.05 carbon dioxide yield (Fig. 3c). The addition of 1 wt% Ni to bare monolith had little to no effect on the product yields. Both bare monolith and 1 wt% Ni/monolith show very poor reforming activity. The addition of nickel from 2–4 wt% resulted in significantly increased hydrogen, carbon monoxide, carbon dioxide, and C_1–C_4 hydrocarbon yields. Slight increases in hydrogen and carbon dioxide yield were observed at weight loadings >4 wt% Ni. The carbon monoxide yield remained relatively constant in the 4–13 wt% Ni range.

The CZO/monolith showed moderate carbon monoxide ($Y_{CO} = 0.09$) and carbon dioxide yields ($Y_{CO_2} = 0.13$), low hydrogen yields ($Y_{H_2} = 0.06$), and significant C_1–C_4 hydrocarbon yields ($Y_{C_1-C_4} = 0.31$). This product spectrum is consistent with a mixture of POX, combustion, and hydrocarbon cracking. Compared with the CZO support alone, the addition of 1 wt% Ni to the CZO support significantly increased the H_2, CO, and CO_2 yields, whereas decreasing the C_1–C_4 yield, indicating that nickel supported on CZO facilitates the conversion of the smaller hydrocarbons into reforming products. Nickel loadings >1 wt% showed a gradual increase in H_2 and CO_2 yields, accompanied by a gradual decrease in CO yield. Nickel loadings >1 wt% Ni led to slightly decreased C_1–C_4 hydrocarbon yields over the Ni/CZO/monolith. The reforming product yields for the Ni/CZO/monolith catalyst were far superior to those of the Ni/monolith catalyst at comparable weight loadings of nickel.

3.5. SR

To gain further insight into the influence of CZO and nickel weight loading on hydrogen generation during ATR, the SR activities of the Ni/monolith and Ni/CZO/monolith were tested under simulated ATR reactor conditions. During the SR reactions, the flow of air was replaced with nitrogen to keep the concentrations of all of the reactants the same as during ATR. The temperature of the furnace was raised to 640 °C to simulate the exotherm associated with POX. A temperature of 640 °C was selected because this was the average exit temperature of the monoliths during the ATR experiments.

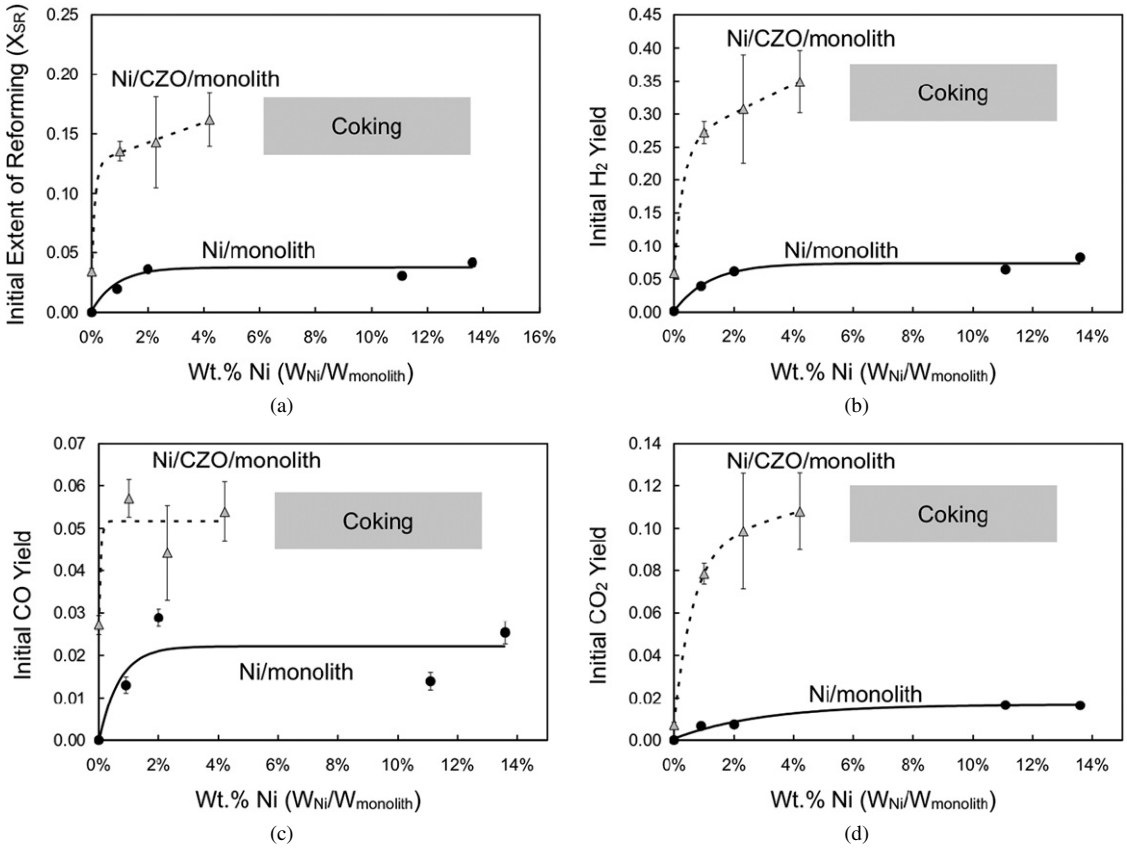

Fig. 4. Steam reforming of *n*-dodecane over Ni/monolith and Ni/CZO/monolith: (a) initial extent of reaction, (b) initial hydrogen yield, (c) initial carbon monoxide yield, (d) initial carbon dioxide yield. Reaction conditions: $H_2O/C = 2.0$, GHSV = 63,000 h^{-1}, feed temp. = 640 °C.

The extent of reforming (X_{SR}) and SR product yields are plotted in Fig. 4. Bare monoliths showed no SR activity. Nickel loadings of 1–2 wt% on the Ni/monolith catalysts led to increased extents of SR and reforming product yields. The addition of >2 wt% nickel had very little influence on the extent of SR and reforming product yields. This behavior is similar to the behavior observed during ATR. In general, the Ni/monolith catalysts (1–14 wt% Ni) had poor SR activity, with yields <0.05. The exit temperature of the Ni/monolith reactor remained constant at 640 °C regardless of nickel loading.

The CZO/monolith showed a small amount of SR activity, with an extent of reforming (X_{SR}) of 0.03, demonstrating that CZO alone had poor SR activity. For the Ni/CZO/monolith catalysts, the extent of reforming and the H_2, CO, and CO_2 yields increased steadily with increasing nickel loading from 1 to 4 wt%, respectively, in marked contrast to the leveling off of performance at 2% nickel loading observed in the Ni/monolith catalysts and also in the ATR experiments. The reactor exit temperatures decreased from 640 to 570 °C, as expected, with increased SR activity. Experiments with nickel loadings >4 wt% were attempted but had to be abandoned due to a rapid buildup of large pressure drops resulting from reactor plugging by carbon deposition. The SR experiments demonstrated that Ni/CZO/monolith catalysts had some *n*-dodecane SR activity at 640 °C and that the Ni/CZO/monolith catalysts were 5–6 times more active than the Ni/monolith catalysts.

3.6. Comparison of POX, SR, and ATR

The behavior of 2 wt% Ni/CZO/monolith and Ni/monolith also were studied under POX conditions to elucidate the nature of ATR and the distinct roles of CZO and nickel. All three reactions and the important performance metrics are compared in Fig. 5. The conversion of *n*-dodecane was nearly identical (∼0.66) for both ATR and POX over both Ni/monolith and Ni/CZO/monolith (Fig. 5a). The conversion of *n*-dodecane by SR alone was significantly lower than the conversion by both POX and ATR, suggesting that POX is a dominant route for *n*-dodecane conversion during ATR. Interestingly, *n*-dodecane conversion by ATR was not the summation of POX and SR conversions, as would be expected were ATR simply the combination of POX and SR. This behavior was different from that of methane ATR, where the conversion of methane was approximately the summation of POX and SR [31]. It cannot be ruled out that the different temperature profiles in the monolith during the three reactions may contribute to the difference in conversion seen in the experiments.

The Ni/CZO/monolith catalyst had a much higher extent of reforming than the Ni/monolith catalyst for all three reactions (Fig. 5b). The extent of SR was greatly improved over the CZO-supported nickel. Clearly, the use of CZO as a support was beneficial for all three reforming reactions. Unlike *n*-dodecane conversion, the extent of ATR ($X_{ATR} = 0.52$) was very similar to the sum of the extents of POX and SR ($X_{POX} + X_{SR} = 0.53$).

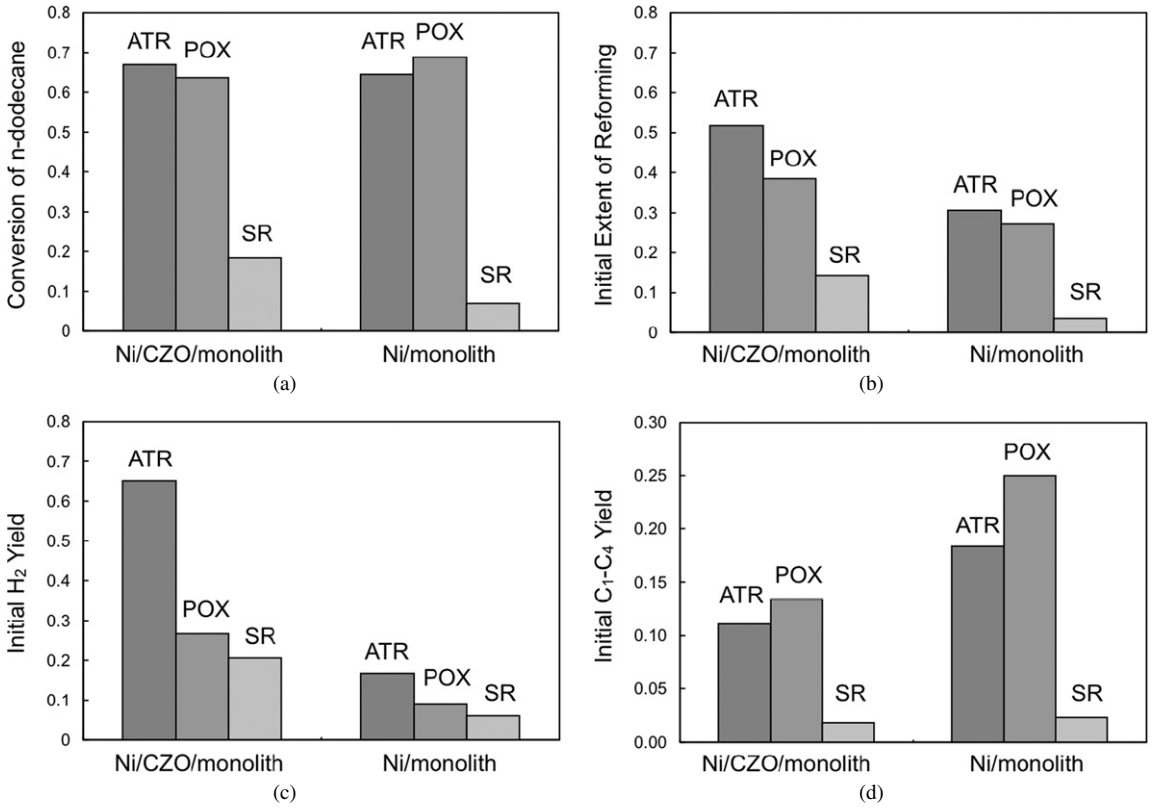

Fig. 5. Comparison of autothermal reforming (ATR), partial oxidation (POX), and steam reforming (SR) over a 2 wt% Ni/CZO/monolith and 2 wt% Ni/monolith: (a) conversion of *n*-dodecane, (b) initial extent of reforming, (c) initial hydrogen yield, (d) initial C_1–C_4 hydrocarbon yield, GHSV = 63,000 h^{-1}, ATR (O/C = 0.6, H_2O/C = 2.0, feed temp. = 550 °C), POX (O/C = 0.6, feed temp. = 550 °C), SR (H_2O/C = 2.0, feed temp. = 640 °C).

This observation is logical because the extent of reforming describes the amount of *n*-dodecane conversion by the specific reforming reaction, and ATR should be similar to the combination of both POX and SR. The *n*-dodecane conversion and extent of reforming demonstrate that, unlike for methane, reforming reactions are not the only possible route for larger hydrocarbon conversion. The other possible carbon-containing products from *n*-dodecane conversion were smaller hydrocarbons, as shown in Fig. 5d. The Ni/monolith catalyst formed larger amounts of cracking products than the Ni/CZO/monolith catalyst in all three reactions, explaining its poorer performance. POX showed the greatest C_1–C_4 hydrocarbon yield over both types of catalysts.

The hydrogen yield during ATR was greater than that during either SR or POX over both types of catalysts (Fig. 5c). This was not surprising, because POX should have a lower hydrogen yield than ATR based on thermodynamics. The lower hydrogen yield in SR can be explained by the fact that under the experimental conditions used here, SR had a lower *n*-dodecane conversion than ATR. For the Ni/CZO/monolith catalyst, the H_2 yield during ATR was 0.65, and the summed H_2 yield during POX and SR was 0.47. The summed SR and POX H_2 yields gave only 70% of the H_2 yield obtained during ATR. This discrepancy may be due to differences in the water–gas shift equilibrium or may reflect a difference in hydrogen selectivity of ATR and its constituent reactions. Overall, the Ni/CZO/monolith material was a superior catalyst for ATR, POX, and SR.

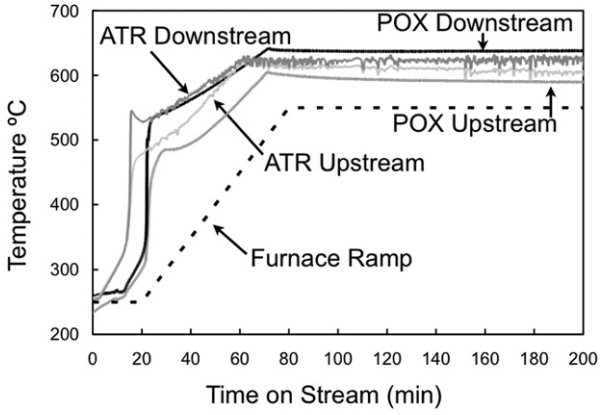

Fig. 6. Temperature–time trajectory for the upstream and downstream thermocouples during partial oxidation and autothermal reforming over 1 wt% Ni/CZO/monolith. Reaction conditions: O/C = 0.6, H_2O/C = 2.0, GHSV = 63,000 h^{-1}, feed temp. = 550 °C.

The time-temperature trajectories during ATR and POX are compared in Fig. 6. ATR showed large temperature oscillations during the course of the reaction, whereas the POX temperature trajectory was very smooth. The upstream and downstream temperatures during POX bracketed the ATR temperatures. The temperature oscillations might be associated with the dynamic interplay of endothermic and exothermic reactions in the monolith under ATR conditions. The possibility that the temperature oscillations are an experimental artifact of water pumping can be ruled out, because the temperature os-

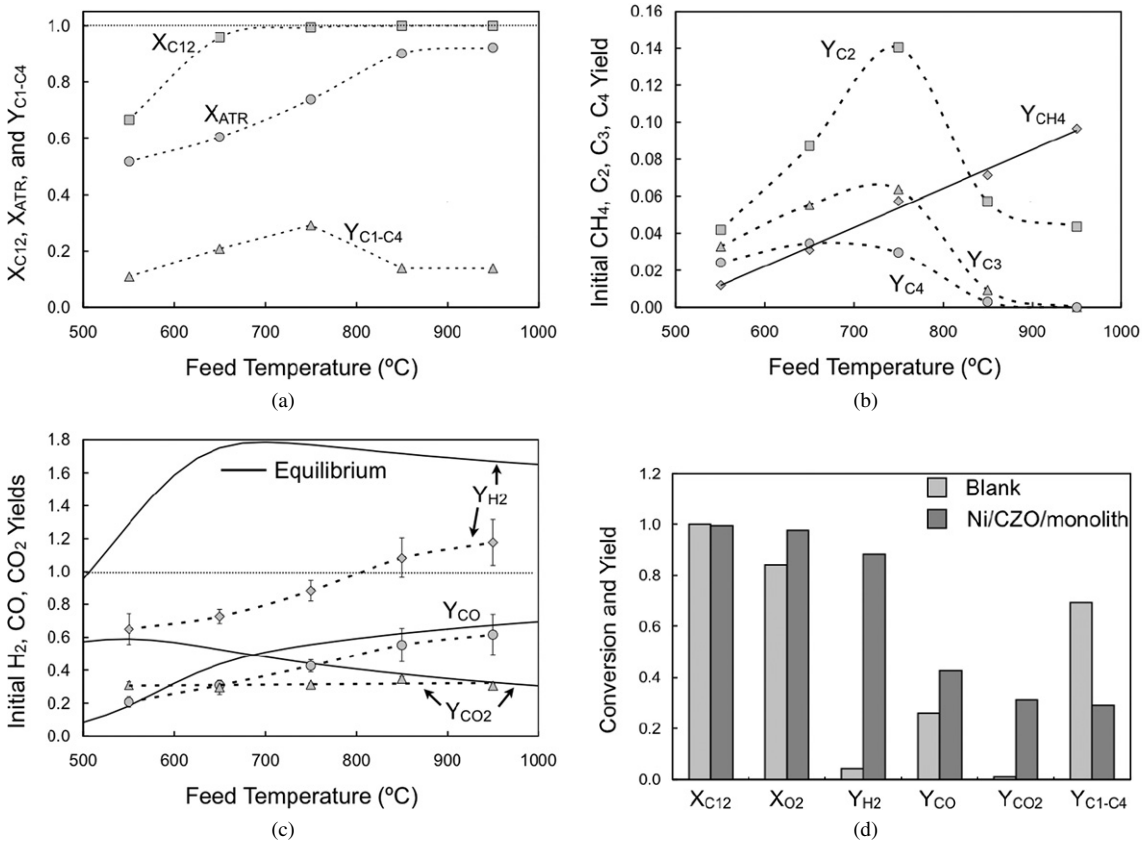

Fig. 7. Autothermal reforming of *n*-dodecane at various feed temperatures over a 2 wt% Ni/CZO/monolith: (a) conversion of *n*-dodecane ($X_{C_{12}}$), extent of reforming (X_{ATR}), and total yield of hydrocarbon species C_1–C_4 ($Y_{C_1-C_4}$), (b) yield of hydrocarbon species C_1–C_4, (c) the initial reforming product yields and equilibrium, (d) blank activity comparison at 750 °C. Reaction conditions: O/C = 0.6, H_2O/C = 2.0, GHSV = 63,000 h^{-1}.

cillations had a much larger period compared with the water pump.

3.7. Influence of temperature on ATR

In the aforementioned experiments, the catalysts were intentionally run under conditions giving incomplete conversion of *n*-dodecane, to allow a meaningful reactivity comparison between the various catalysts. The influence of temperature on product yields and conversion was studied to provide a basis for future optimization of *n*-dodecane reforming. The 2 wt% Ni/CZO/monolith catalysts were tested for ATR activity over a range of feed temperatures (550–950 °C); the results are shown in Fig. 7. At a feed temperature of 550 °C, the conversion of *n*-dodecane ($X_{C_{12}}$) was 0.67. As the feed temperature was increased from 550 to 650 °C, *n*-dodecane conversion increased to 0.96. From 750 to 950 °C, the *n*-dodecane was completely converted. Interestingly, the extent of ATR (X_{ATR}) was lower than the overall *n*-dodecane conversion ($X_{C_{12}}$) and did not trace the *n*-dodecane conversion trend with increasing feed temperature. Whereas the *n*-dodecane conversion leveled off at near 100% at 750 °C, the extent of reforming increased steadily, leveling off at 850 °C. The difference between the *n*-dodecane conversion curve and the extent of ATR curve represents the amount of carbon not ending up in CO and CO_2 products. The carbon balance is closed by C_1–C_4 hydrocarbons, the yield of which increased above 550 °C and reached a maximum at 750 °C. Above 750 °C, the C_1–C_4 hydrocarbon yield decreased and leveled off. It is important to note that above 850 °C, the C_1–C_4 yield was composed mainly of methane, the most stable hydrocarbon, whereas at lower temperatures, C_2–C_4 products were more prominent. The C_1–C_4 product distribution as function of feed temperature is shown in Fig. 7b.

The trends in reforming product yields and theoretical equilibrium yields as a function of temperature are shown in Fig. 7c. Theoretical equilibrium yields were calculated from the total molar flow rate and product distributions determined by Gibbs free energy minimization. Gibbs free energy minimization calculations were performed with the commercial software package ASPEN™ and accounted for the possible production of the following hydrocarbons: *n*-dodecane, methane, ethane, ethylene, propane, and propylene. Hydrogen and carbon monoxide yields showed a similar trend with increasing temperature. Both yields gradually increased from 650 to 950 °C. Hydrogen yields >1.0 were observed at 850 °C. The carbon dioxide yield remained constant over the range of temperatures tested. Increased feed temperatures led to increased reforming product yield though the SR of the smaller hydrocarbons. Comparing the experimental yields with the predicted yields from chemical equilibrium shows that in the experimental yields, equilibrium was never reached during ATR at the temperatures examined. At low temperatures, the departure from equilibrium can be

explained by incomplete conversion of *n*-dodecane. At higher temperatures, the carbon monoxide and carbon dioxide yields approached equilibrium, but hydrogen yields remained significantly lower than the predicted equilibrium. Equilibrium predicted only trace levels of hydrocarbons larger than methane. But experimentally, significant portions of the hydrogen atoms were present in C_2–C_4 hydrocarbons, thus accounting for the lower hydrogen yield over the catalysts (Fig. 7c).

Blank quartz tube experiments carried out at 750 °C, the temperature at which complete *n*-dodecane conversion was achieved in presence of catalyst, demonstrated that complete *n*-dodecane conversion was achieved even in the absence of catalyst. But the product distribution was strikingly different in the blank runs, with very low H_2 and CO_2 yields (Fig. 7d) but significant C_1–C_4 yields. This suggests that at elevated temperatures, homogeneous POX and cracking reactions contributed to the *n*-dodecane conversion. The low hydrogen yields are likely the result of homogeneous hydrogen oxidation. This hypothesis is supported by the finding that not all of the converted oxygen ended up in the form of carbon monoxide. The only other possible oxygen-containing products would be water or oxygenates, but the former could not be quantified in the gas chromatograph, and no evidence for the latter was observed.

Ultimately, the selection of fuel processor operating conditions depends on the application. Under our reaction conditions, which have intentionally low oxygen-to-carbon ratios, the best ATR product yields were observed at 950 °C. However, significant amounts of methane (2.8 mol%) remained even at these high temperatures. In solid oxide fuel cells capable of utilizing methane, significant amounts of methane actually would be beneficial in terms of fuel value. If methane is an undesirable product, then the oxygen-to-carbon ratio can be used to mitigate the methane yield. A temperature of 950 °C would be impractical for many applications, and different reactor conditions, such as O/C, would need to be optimized, depending on the application.

3.8. Role of nickel and CZO

The nickel in the Ni/CZO/monolith and Ni/monolith catalysts has two functions. Nickel can catalyze the POX of *n*-dodecane, as demonstrated by the observation that increased nickel loadings caused increased oxygen and *n*-dodecane conversion (Fig. 2a). Nickel also can catalyze hydrocarbon SR. Nickel's ability to catalyze hydrocarbon reforming is supported by both the SR and ATR data. The SR data show that the addition of nickel to bare monolith or CZO-coated monolith increases SR product yields (H_2, CO, and CO_2). The ATR data show that nickel increases reforming product yields while consuming smaller hydrocarbons when supported on CZO. Nickel's ability to catalyze both POX and SR of large hydrocarbons is consistent with previous reports [35,36].

CZO alone is an active but nonselective hydrocarbon oxidation catalyst capable of complete oxygen conversion, as shown in Fig. 2b. Although over CZO/monolith, the oxygen conversion is complete and the *n*-dodecane conversion is equivalent

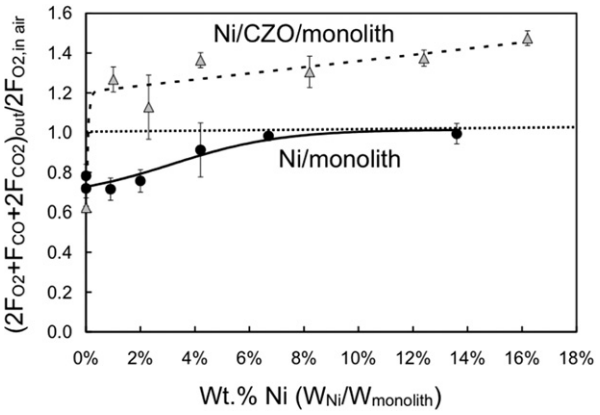

Fig. 8. Partial oxygen balance comparing the oxygen atoms in the products to the oxygen atoms in the air feed during autothermal of *n*-dodecane over Ni/CZO/monolith and Ni/monolith, reactor conditions: O/C = 0.6, H_2O/C = 2.0, GHSV = 63,000 h^{-1}, feed temp. = 550 °C.

to catalysts containing nickel, the major products are carbon monoxide, carbon dioxide, and smaller hydrocarbons. The large carbon monoxide and carbon dioxide yields with the low hydrogen yields suggest that some combination of partial and deep oxidation is occurring over the CZO. We propose that the catalytic role of CZO in the catalyst is to act as a site for oxidation and to break the *n*-dodecane down into smaller hydrocarbon species.

The most striking difference between Ni/CZO/monolith and Ni/monolith catalysts is their respective hydrogen yields (Fig. 3a). One possible explanation for the different hydrogen yields at the same *n*-dodecane conversions is that nickel supported on CZO is promoting the participation of water in the reaction. The ability of nickel supported on CZO to promote the participation of water in the reaction can be visualized by plotting a fractional oxygen balance for the reaction. The fractional oxygen balance is defined as the ratio of the flow of oxygen atoms in the products to the flow of oxygen atoms associated with the air feed. The fractional oxygen balance neglects oxygen atoms present in water as a feed or as a product and is shown in Fig. 8. A ratio greater than unity means that water participated in the oxidation of carbon contained in the fuel either through a water–gas shift of carbon monoxide produced during POX or SR of the *n*-dodecane or through SR of the *n*-dodecane cracking products. A fractional oxygen balance <1 does not necessarily mean that water did not participate in the reaction, but rather that oxygen in the air reacted to form water as a product. Bare monoliths showed a fractional oxygen balance of 0.72. With increased nickel loadings of the Ni/monolith, the fractional oxygen balance gradually increased and leveled off at values slightly below unity at the higher nickel loadings. The nickel-free CZO coated monolith showed the lowest fractional oxygen balance, most likely due to hydrogen being oxidized to water, which is consistent with the low hydrogen yields discussed earlier (Fig. 3a). But as soon as 1 wt% nickel was added to the CZO-coated monolith, the fractional oxygen balance jumped beyond unity. With higher nickel loadings, the fractional oxygen balance increased even further.

The fractional oxygen balance data and the other observations reported earlier strongly support the notion that one role of the CZO support is to promote the participation of water in ATR. Ceria's ability to promote the SR of methane through a redox mechanism is currently a topic of debate [10,37]. Unfortunately, most of the mechanistic work has been performed on methane, and the analogy between methane and higher hydrocarbons is tentative at best, because methane proceeds though carbon–hydrogen bond activation, whereas higher hydrocarbons are proposed to proceed through α-scission of carbon–carbon bonds, followed by adsorbed C_1 species reaction with steam [38]. It seems plausible that ceria may promote participation of water in SR through a redox mechanism for higher hydrocarbons, and a metal–support interaction has been postulated for larger hydrocarbons [18,39]. Careful kinetic studies are needed to determine the precise mechanism and the kinetic relevance of the ceria support. Whereas our reaction data clearly show that the use of CZO as a support increases the participation of water in the ATR reaction, our catalyst characterization data also show that the CZO support increases the total surface area and the dispersion of nickel by a factor of 3 (Tables 1 and 2). Our experiments were not designed to probe mechanistic details, and we cannot separate the mechanistic contribution of CZO from dispersion or support interaction effects. However, from a macroscopic viewpoint, there is no doubt that the use of CZO as a support in monolith catalysts is beneficial.

The ratio of reforming product yields to used nickel is maximized at nickel loadings between 1 and 2 wt% Ni for the Ni/CZO/monolith catalysts. Although the higher nickel loadings lead to slight improvements in hydrogen yield, these gains in hydrogen are generally offset by the decreased carbon monoxide yield. For this reason, we believe that the 2 wt% Ni/CZO/monolith catalyst represents the optimal catalyst composition for auxiliary power unit applications.

3.9. Interpretation of ATR results

The experimental evidence gathered in our work indicates that ATR of larger hydrocarbons is more complex than simply the combination of POX and SR. In fact, our observations of significant amounts of C_1–C_4 reaction products under ATR conditions show that some of the *n*-dodecane undergoes cracking to C_1–C_4 products. Our feed temperature of 550 °C is high enough to cause homogeneous thermal and/or oxidative cracking, or heterogeneous cracking. In fact, when *n*-dodecane and air were fed at 550 °C though a blank monolith, about 40% of the *n*-dodecane underwent thermal cracking or homogeneous oxidation reactions. Under our ATR conditions, the thermal environment encountered by *n*-dodecane approaching the Ni/CZO/monolith is even more severe, due to additional radiative heat transfer from the much hotter entrance segment of the monolith, where highly exothermic POX reactions are occurring. We believe that it is in this hot entrance section to the catalyst where most of the *n*-dodecane conversion occurs through POX and further cracking. Once oxygen is exhausted, the smaller hydrocarbon fragments generated and the remaining *n*-dodecane and steam reach the downstream section of the monolith, where SR becomes dominant. A qualitative depiction of the types of reactions participating under *n*-dodecane ATR conditions is presented in Fig. 9. Bold arrows represent the primary routes to reforming products, and the thin arrows represent minor routes. We propose that POX is the major route for *n*-dodecane conversion, with oxidative cracking occurring because of a sub-stoichiometric amount of oxygen (O/C = 0.6). POX of *n*-dodecane and SR of smaller hydrocarbons produced from cracking are the two primary routes to reforming products (CO and H_2). An equilibrium mixture of carbon monoxide, carbon dioxide, and hydrogen is produced through water–gas shift equilibrium.

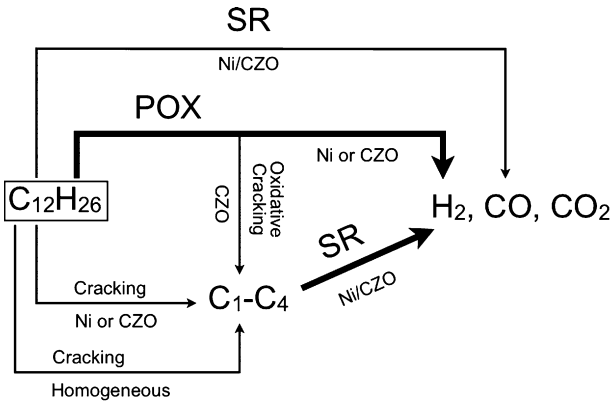

Fig. 9. Schematic of postulated autothermal reforming routes with possible homogeneous and catalytic cracking contributions. Note that water–gas shift is not explicitly shown in this schematic, but is implied by the H_2, CO, and CO_2 product mix.

Catalytic POX is evident from the dependence of oxygen conversions on nickel loading and the observation that complete oxygen conversion was achieved only in the presence of a catalyst (Fig. 2a). The trends in hydrogen, carbon monoxide, and carbon dioxide yields over the Ni/CZO/monolith are all consistent with a contribution from SR plus the water–gas shift reaction (Figs. 3a–3c). The water–gas shift reaction is often considered equilibrated under reforming conditions, and ceria is a known water–gas shift promoter at low temperatures [40–42]. One possible interpretation of the ATR data is that SR acts primarily on the smaller hydrocarbons rather than on *n*-dodecane. It has been postulated by Qi et al. [43] that *n*-octane ATR goes though methane and short-chain hydrocarbon intermediates. Under our ATR conditions with complete oxygen conversion, increased Ni loadings in both the Ni/monolith and Ni/CZO/monolith catalysts did not lead to increased *n*-dodecane conversion by the only other remaining reactant, H_2O (Figs. 2a and 2b). This trend is counterintuitive, because nickel is a good SR catalyst. If POX was responsible for the majority of *n*-dodecane conversion and SR acted only on the smaller hydrocarbons produced during POX, then the constant *n*-dodecane conversion could be rationalized.

This SR mechanism is further supported by the high-temperature ATR work, in which the difference between *n*-dodecane conversion and the extent of reforming was accounted for by the formation of smaller hydrocarbons. With increasing temperature, the smaller hydrocarbons were converted into

CO and H_2 by SR. The hydrocarbon yields of individual carbon numbers (Fig. 7b) showed that as the temperature was increased, the C_2–C_4 hydrocarbons were converted by SR, and methane was formed. It is our belief that the likely source of methane is the splitting of larger hydrocarbons into methane; however, there are two other plausible routes for methane formation: methanation of the carbon monoxide and hydrogen present, and hydrogenation and/or hydrogenolysis of the adsorbed C_xH_y moieties. Methanation has been shown to occur over nickel catalysts at 250 °C [44,45]. Methanation is an exothermic reaction that should be thermodynamically favored by lower temperatures and high pressures, not by the high temperatures and low pressures of ATR. On the other hand, nickel is a well-known hydrogen-transfer catalyst, and it is conceivable that the C_2–C_4 products undergo hydrogenation and subsequent hydrogenolysis reactions [46]. Hydrogenolysis reactions are endothermic and should be favored at higher temperatures. The source of methane at high temperatures remains open to speculation, but hydrogenation/hydrogenolysis of the smaller hydrocarbon species seems to be thermodynamically more probable.

To gain more insight into the validity of our postulated *n*-dodecane ATR schematic, we explored the contribution of SR by operating the reactor under conditions analogous to the ATR runs, with the only difference being the replacement of oxygen with nitrogen. The exotherm encountered during ATR was approximated by an additional electric heat supply. Comparing the SR, ATR, and POX *n*-dodecane conversions (Fig. 5a) shows that the Ni/monolith catalysts had low SR activity, consistent with the above ATR schematic. However, the SR results over Ni/CZO/monolith under these simulated "autothermal" conditions showed moderate *n*-dodecane conversion, inconsistent with the postulate that direct SR of *n*-dodecane is not a major route during ATR. This discrepancy might be attributable to the difference in reaction environments. Although great care was taken to try to make the two reaction environments as similar as possible, there was no way to fully duplicate the reactant, product, and temperature profiles in the monolith.

Whereas our postulated ATR schematic explains our experimental findings for *n*-dodecane over Ni and Ni/CZO catalysts, at this point it cannot be generalized for all liquid hydrocarbons, particularly aromatics and branched hydrocarbons. Aromatic compounds are much more stable than normal alkanes and should exhibit far less homogeneous cracking at a given temperature.

4. Conclusion

The Ni/CZO/monolith catalysts had greater ATR product yields than the Ni/monolith catalysts. CZO on monolith without nickel was capable of complete oxygen conversion, but with poor selectivity toward ATR products. Adding nickel to the CZO support led to significant improvements in ATR product yields. Nickel acted as a site for both POX and SR. Marginal gains in product yield were realized with large nickel weight loadings. The optimal nickel loading for the Ni/CZO/monolith catalyst was 2 wt%. The benefit of using CZO as support in the Ni/CZO/catalyst was increased participation of water in ATR though SR. Whether this benefit stems from increased nickel dispersion and surface area or from a metal–support interaction remains unresolved.

ATR of *n*-dodecane showed significant conversion of *n*-dodecane through homogeneous chemistries under these conditions, especially at elevated temperatures. At 550 °C, the conversion on *n*-dodecane was limited by the conversion of oxygen on all nickel-containing catalysts, suggesting that POX was the primary route for *n*-dodecane conversion at low temperatures. *n*-Dodecane ATR involves a complex set of reactions, including thermal cracking of *n*-dodecane, homogeneous and heterogeneous oxidation of *n*-dodecane and the smaller hydrocarbons formed, SR of *n*-dodecane and the smaller hydrocarbons, and the water–gas shift. The contribution of SR to the conversion of smaller hydrocarbons formed during ATR of *n*-dodecane is consistent with most of our results. The conversion of *n*-dodecane can be increased by raising the operating temperature, but then the formation of smaller hydrocarbons, particularly methane, becomes more pronounced with increased feed temperatures. Within the parameter space explored in this work, ATR gave superior reformate yields compared to both SR and POX.

Acknowledgments

Financial support was provided by the U.S. Army Tank-Automotive Research, Development & Engineering Center under cooperative agreement W56HZV-05-2-0001. The authors thank master glassblower Harald Eberhart for his skillful fabrication of the quartz reactors and Joseph Mayne for his helpful collaboration with reaction experiments.

References

[1] J.G. Buglass, M.F. Goes, R.J. Schoonebeek, PCT Int. Patent Appl. 2005029629 (2005), to Shell International Research.
[2] W.J. LaBarge, J. Kupe, G.B. Fisher, J.E. Kirwan, R.M. Rahmoeller, US Patent Appl. 20040086432 (2005), to Delphi Technologies Inc.
[3] S. Jain, H. Chen, J. Schwank, J. Power Sources 160 (2006) 474.
[4] R.M. Heck, R.J. Farrauto, Catalytic Air Pollution Control, Van Nostrand Reinhold, New York, 1995, p. 77.
[5] S. Ahmed, M. Krumpelt, Int. J. Hydrogen Energy 26 (2001) 291.
[6] S.H.D. Lee, D.V. Applegate, S. Ahmed, S.G. Calderone, T.L. Harvey, Int. J. Hydrogen Energy 30 (2005) 829.
[7] J. Larminie, A. Dicks, Fuel Cell Systems Explained, second ed., Wiley, London, 2003, p. 249.
[8] S. Springmann, G. Friedrich, M. Himmen, M. Sommer, G. Eigenberger, Appl. Catal. A 235 (2002) 101.
[9] H.S. Bengaard, J.K. Nørskov, J. Sehested, B.S. Clausen, L.P. Nielsen, A.M. Molenbroek, J.R. Rostrup-Nielsen, J. Catal. 209 (2002) 365.
[10] J. Wei, E. Iglesia, J. Phys. Chem. B 108 (2004) 4094.
[11] D.A. Hickman, L.D. Schmidt, AIChE J. 39 (1993) 1164.
[12] I. Tavazzi, A. Beretta, G. Groppi, P. Forzatti, J. Catal. 241 (2006) 1.
[13] Y. Boucouvalas, Z.L. Zhang, A.M. Efstathiou, X.E. Verykios, Stud. Surf. Sci. Catal. 101 (1996) 443.
[14] D. Shekhawat, D.A. Berry, T.H. Gardner, J.J. Spivey, Catalysis 19 (2006).
[15] J.A.S. Bett, M.C. Cutlip, P.F. Foley, R.R. Lesieur, A.P. Meyer, R.A. Sederquist, H.J. Setzer, Fuel processing for fuel cells: A model for fuel

conversion and carbon formation in the adiabatic steam reformer, Report by United Technologies Power Systems (1983).
[16] M. Flytzani-Stephanopoulos, G.E. Voecks, Int. J. Hydrogen Energy 8 (1983) 539.
[17] M. Krumpelt, T.R. Krause, J.D. Carter, J.P. Kopasz, S. Ahmed, Catal. Today 77 (2002) 3.
[18] R.M. Navarro, M.C. Alvarez-Galvan, F. Rosa, J.F.G. Fierro, Appl. Catal. A 297 (2006) 60.
[19] D. Liu, T.D. Kaun, H. Liao, S. Ahmed, Int. J. Hydrogen Energy 29 (2004) 1035.
[20] R.L. Borup, M.A. Inbody, T.A. Semelsberger, J.I. Tafoya, D.R. Guidry, Catal. Today 99 (2005) 263.
[21] P.K. Cheekatamarla, A.M. Lane, J. Power Sources 153 (2006) 157.
[22] D. Liu, T.D. Kaun, H. Liao, S. Ahmed, Int. J. Hydrogen Energy 29 (2004) 1053.
[23] C. Palm, P. Cremer, R. Peters, D. Stolten, J. Power Sources 106 (2002) 231.
[24] Q. Ming, T. Healey, L. Allen, P. Irving, Catal. Today 77 (2002) 51.
[25] T. Suzuki, H. Iwanani, T. Yoshinari, Int. J. Hydrogen Energy 25 (2000) 119.
[26] J. Hu, Y. Wang, D. VanderWiel, C. Chin, D. Palo, R. Rozmiarek, R. Dagle, J. Cao, J. Holladay, E. Baker, Chem. Eng. J. 93 (2003) 55.
[27] W.-S. Dong, K.-W. Jun, H.-S. Roh, Z.-W. Liu, S.-E. Park, Catal. Lett. 78 (2002) 215.
[28] D. Shekhawat, T.H. Gardner, D.A. Berry, M. Salazar, D.J. Haynes, J.J. Spivey, Appl. Catal. A 311 (2006) 8–16.
[29] J.M. Kuchta, Investigation of fire and explosion accident in the chemical, mining, and fuel-related industries—A manual, Bulletin 680, U.S. Bureau of Mines, 1985.
[30] B.D. Gould, A.R. Tadd, J.W. Schwank, J. Power Sources 164 (2007) 344.
[31] T. Giroux, S. Hwang, Y. Liu, W. Ruettinger, L. Shore, Appl. Catal. B 56 (2005) 95.
[32] P.K. Cheekatamarla, A.M. Lane, J. Power Sources 152 (2005) 256.
[33] B. Gould, Doctorial dissertation, University of Michigan, 2007.
[34] R.K. Kaila, A.O.I. Krause, Int. J. Hydrogen Energy 31 (2006) 1934.
[35] S. Pengpanich, V. Meeyoo, T. Rirksomboon, J. Schwank, Appl. Catal. A 302 (2006) 133.
[36] D. Duprez, Appl. Catal. A 82 (1992) 111.
[37] R. Craciun, B. Shereck, R.J. Gorte, Catal. Lett. 51 (1998) 149.
[38] J.R. Rostrup-Nielsen, Catalytic Steam Reforming, vol. 5, Springer-Verlag, 1984, chap. 1, p. 55.
[39] K. Polychronopoulou, C.N. Costa, A.M. Efstathiou, Catal. Today 112 (2006) 89.
[40] C. Wheeler, A. Jhalani, E.J. Klien, S. Tummala, L.D. Schmidt, J. Catal. 223 (2004) 191.
[41] B.I. Whittington, C.J. Jiang, D.L. Trimm, Catal. Today 26 (1995) 41.
[42] X. Wang, R.J. Gorte, Appl. Catal. A 247 (2003) 157.
[43] A. Qi, S. Wang, G. Fu, D. Wu, Appl. Catal. A 293 (2005) 71.
[44] J. Sehested, S. Dahl, J. Jacobsen, J.R. Rostrup-Nielsen, J. Phys. Chem. B 109 (2005) 2432.
[45] A.E. Zagli, J.L. Falconer, C.A. Keenan, J. Catal. 56 (1979) 453.
[46] G.A. Somorjai, Introduction to Surface Chemistry and Catalysis, Wiley, New York, 1994, p. 557.